Russian Journal of Earth Sciences

Features of Long Waves in the Area of Cape Svobodny (South-Eastern Part of Sakhalin Island, Russia) During the Passage of Cyclones

Andrey Kurkin*[,1], Dmitry Kovalev[2], Oxana Kurkina[1] and Peter Kovalev[2]

[1] Nizhny Novgorod State Technical University n.a. R. E. Alekseev, Nizhny Novgorod, Russia
[2] Institute of Marine Geology and Geophysics Far Eastern Branch Russian Academy of Sciences, Yuzhno-Sakhalinsk, Russia
* **Correspondence to:** Andrey Kurkin, aakurkin@gmail.com

Abstract: The study of marine wave processes was carried out according to field observations using two autonomous wave recorders, temperature and weather station installed near Cape Svobodny, south-east coast of Sakhalin (Russia). Spectral and cross-spectral analysis showed the existence of edge waves with a period of about 10.7 min. Measurements in 2021 showed that the edge wave existing from Cape Ostry to Cape Svobodny, just beyond the cape Svobodny significantly weakens and does not spread further. The analysis of temperature fluctuations for the period range 1–80 hours showed that since the periods of spectral density peaks of water temperature fluctuations for periods longer than 5 hours do not coincide with the periods of peaks of sea level fluctuations, these peaks are determined by internal waves. Temperature fluctuations with a period of 25.5 hours detected by peaks in the spectra can be excited by shelf waves with the same period because of their interaction with islands, coastal currents and baroclinic instability. The analysis of cyclone wakes based on the time course of temperature fluctuations made it possible to establish that cyclone wakes are formed when the water temperature of the upper mixed layer exceeds 10 °C, and internal waves with a period of about 13 hours are also present when cyclones do not move near the point of installation of devices and the water temperature is below 10 °C. The Burger number is determined, which makes it possible to correct the range of existence near inertial internal waves and determine this range periods of 12.1–18.2 hours. Using the results of a simple linear Phillips model, the possibility of baroclinic instability for periods of shelf waves is estimated. It is shown that baroclinic instability is possible for waves with a period of 13.1 hours, and even more so for shelf waves with a significantly longer wavelength.

Keywords: internal waves; Burger number; baroclinic instability

Citation: Kurkin, A., D. Kovalev, O. Kurkina, and P. Kovalev (2023), Features of Long Waves in the Area of Cape Svobodny (South-Eastern Part of Sakhalin Island, Russia) During the Passage of Cyclones, *Russ. J. Earth. Sci.*, 23, ES3003, https://doi.org/10.2205/2023es000852

Research Article

Received: 24 April 2022
Accepted: 5 May 2023
Published: 31 July 2023

1. Introduction

The Laboratory of Wave Dynamics and Coastal Currents of the Institute of Marine Geology and Geophysics of the Far Eastern Branch of the Russian Academy of Sciences has been monitoring waves in various places of the coastal zone of Sakhalin Island and the Kuril Islands (Russia) for many years in order to clarify the features of the wave regime, since it is known that for each specific water area, waves manifest themselves differently and there may be different types of waves, such as seiches, which can intensify during the

passage of storms, as well as infragravity, edge and reflected waves. All of them relate to surface gravity waves.

Although the focus of the paper is on cyclone wakes, the paper briefly discusses several other types of waves, such as tidal, shelf and edge waves. It is known that tidal waves are formed mainly due to the influence of the gravitational forces of the sun and moon. A large number of papers and books are devoted to tidal waves. The most general and complete can be attributed to the book [*Parker*, 2007].

Continental shelf waves are formed in the shelf – continental slope zone as a result of the combined effect of the variability of the relief and the rotation of the Earth. They are a consequence of the law of conservation of the potential vortex [*Kamenkovich*, 1973] – the gradient of the potential vortex provides the possibility of low-frequency oscillations on the shelf. Shelf waves exist at frequencies below the inertial frequency and are the most important type of low-frequency topographic oscillations that play a significant role in the formation of synoptic fluctuations in ocean level and coastal currents, topographic vortices, sedimentary material transfer, formation of daily tides, etc. [*Mysak*, 1980a; *Rabinovich*, 1984]. Edge waves differ from shelf waves in shorter periods and can exist even in the absence of rotation of the Earth, since by their nature they are gravitational. The trapped of edge waves is associated with the effect of total internal reflection (from the shelf boundary), well known in optics [*Efimov et al.*, 1985].

Internal waves with frequencies close to the local inertial frequency have been observed by many researchers in different oceans and at different depths [*Alford*, 2003; *Alford et al.*, 2016; *D'Asaro*, 1985; *Guan et al.*, 2014; *Pollard and Millard*, 1970; *Sanford et al.*, 2011; *Yang et al.*, 2015]. They are usually considered in connection with the wakes of hurricanes – internal waves formed after the passage of a hurricane. And the observations used usually relate to single hurricane, which, as noted in [*Price*, 1983], differ from cyclones of the middle latitudes, following a succession. At the same time, the study of internal waves, and, in particular, near-inertial (NI) waves, is of interest because they support the thermohaline circulation of the ocean, affect the climate [*Alford*, 2003] and contribute to significant mixing of the ocean, and, as a result, the dispersion of pollutants and the improve the productivity of the sea [*Alford*, 2003; *Gregg*, 1987; *Price*, 1981].

In the water area near Cape Svobodny, the southeastern part of the Sakhalin Island in 2020 an experiment was conducted to compare data obtained using wave meters with various primary pressure transducers. The received recordings of waves were analyzed and showed the presence of so-called wakes of cyclones – internal waves with near-inertial frequency that occur after the passage of cyclones. The results of the study of this phenomenon were considered in the paper [*Kovalev et al.*, 2022].

It was decided to continue studying wave processes in the area of Cape Svobodny, and two ARV 14 K devices (autonomous wave recorder) were installed in 2021 [https://sktbelpa.ru/produktsiya-ru/preobrazovateli-absolutnogo-davleniya-i-temperatury-s-tsifrovym-vykhodnym-signalom.html]. Map of the southern part of Sakhalin Island, water area of Mordvinova Bay and Cape Svobodny with the location of the wave and temperature meters are shown in Figure 1. The installation depth of the device number 149 was about 14 meters, and the device number 150 was about 12 meters. The distance between the devices is 1.526 km, according to the isobate 1.69 km. The device, installed in 2020, was located at a same point with device number 150, but almost 4 meters deeper. All instruments recorded fluctuations in sea level and temperature with a 1-second discreteness.

2. Observational data

As a result of the observations, five-month records of sea level fluctuations and water temperature with one second discreteness were obtained, which are shown in Figure 2a,b. About a month after the start of wave registration on July 9, 2021, a Vantage Pro2™ weather station was installed at the lighthouse at Cape Svobodny, which recorded atmospheric pressure and wind speed with a resolution of 1 hour. During the observations, the atmospheric

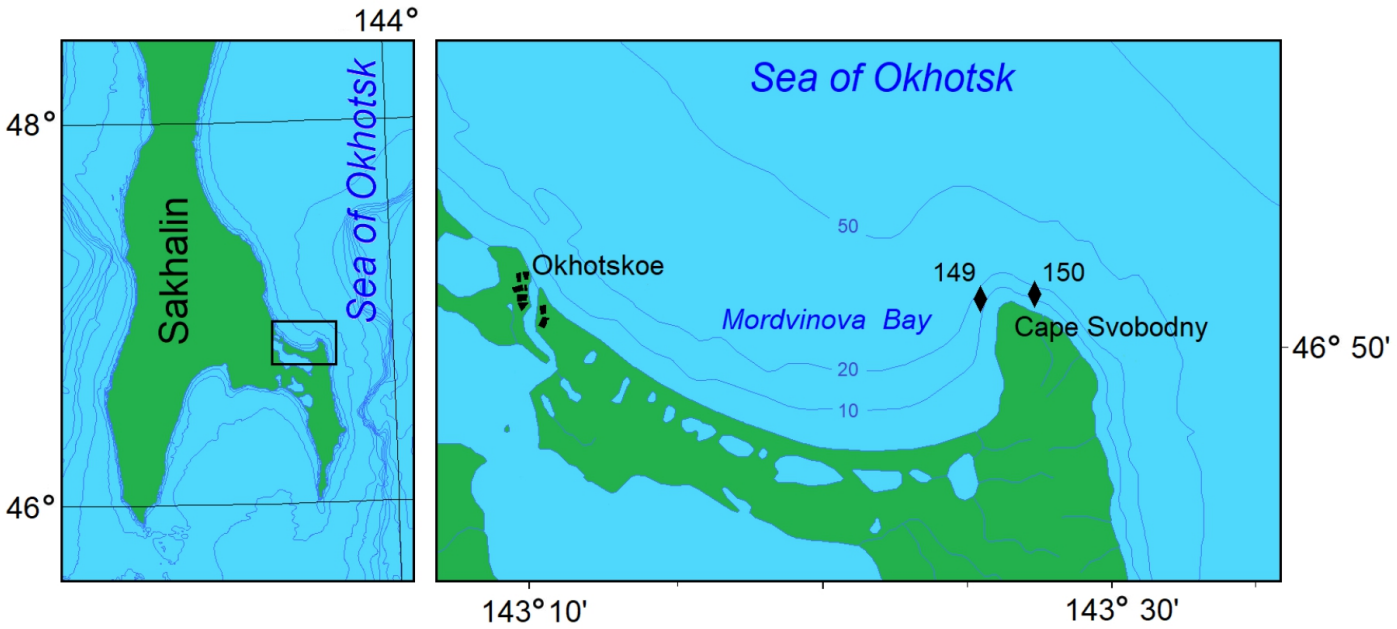

Figure 1. Map of the southern part of Sakhalin Island, water area of Mordvinova Bay and Cape Svobodny with the location of wave and temperature meters.

pressure ranged from 750 to 770 mmHg. The decrease in atmospheric pressure is often associated with southerly winds. The dynamics of pressure fluctuations increases in the autumn period with the arrival of frequent storms.

The time series of atmospheric pressure and wind speed is also shown in Figure 2c,d.

The time series of sea level fluctuations shows tidal waves and several storms with the strongest in mid-September, when the wave height reached 4 m. Also note that frequent storms were observed in the autumn months (September and October). It is clearly seen from the comparison of Figure 2a and Figure 2d that these strong storms are accompanied by strong northerly winds. In this area the predominance of alongshore winds of the north and south directions is visible due to the high mountains along the coast of Sakhalin – at Cape Svobodny the Tonino-Anivsky ridge begins with a mountain height of up to 504 m.

According to the records of water temperature fluctuations (Figure 2b), temperature fluctuations recorded by the device 150 are visible; they are higher frequency than for the device 149. Perhaps this is due to the fact that the device 149 was slightly covered by the Cape Svobodny from the waves of the southern direction. In June–July, fluctuations in water temperature generally did not exceed 8 °C. But in the middle and at the end of August, there are prolonged temperature rises, and in mid-September, with the arrival of a strong cyclone, the water temperature rises sharply to about 14 °C and then begins to slowly decrease.

3. Analysis of sea level fluctuations

Spectral and cross-spectral analysis of time series of sea level fluctuations was carried out using the Kyma program [*Kovalev*, 2018; *Plekhanov and Kovalev*, 2016], which allows processing time series of long duration and volume. The program is designed to process oceanographic data: time series of waves, water temperature, current velocity and other time series. The program allows to prepare the observed data (subtract the tide, restore the true wave heights, correct errors) and perform their spectral and cross-spectral analysis, calculate spectrograms, as well as arrange the results of processing and analysis in the form of images.

The calculated diagram of the spectral density of the wave energy in the range of periods of wind waves, swell and infragravity waves is shown in Figure 3. It can be seen that the spectrum of wind waves and swell has a fairly smooth rise with a maximum of

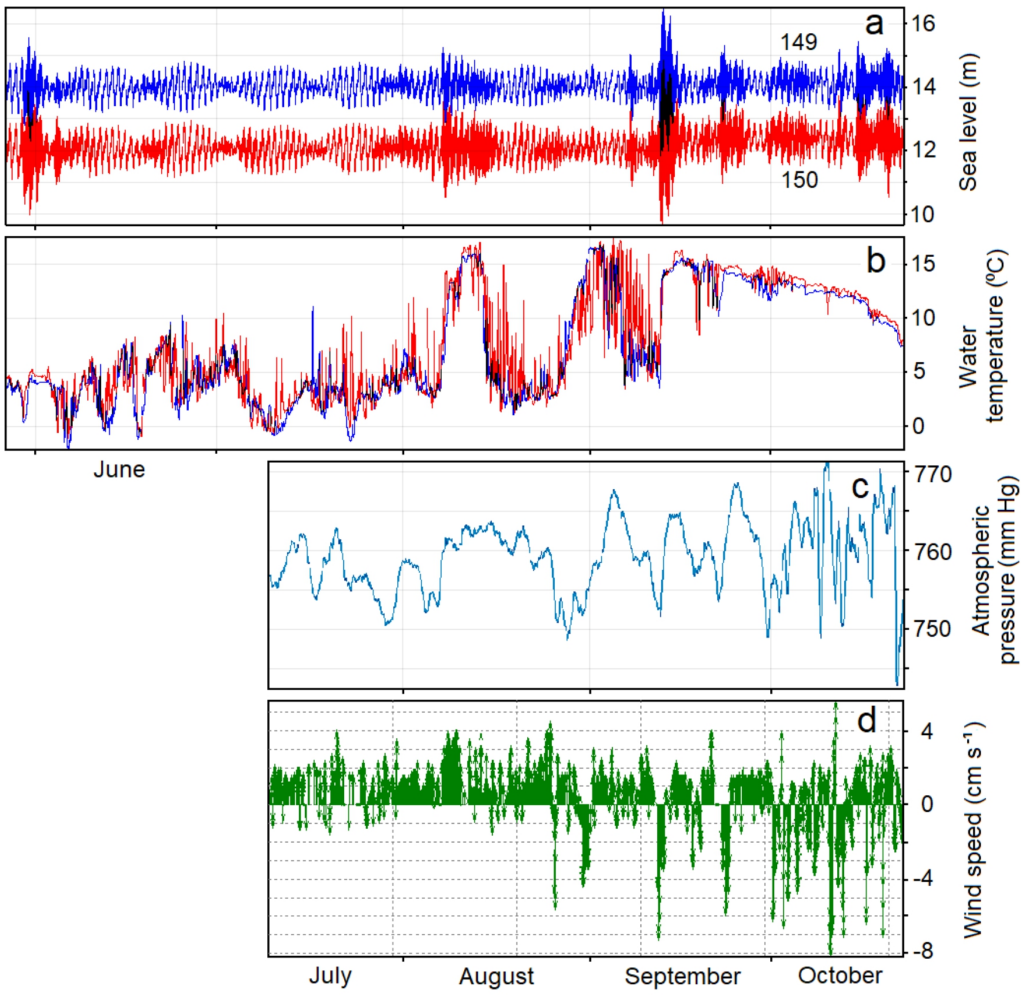

Figure 2. The time series of sea level and water temperature fluctuations (a, b) recorded by devices 149 and 150. The time series of atmospheric pressure and wind speed fluctuations (c, d) registered by the Vantage Pro2™ weather station in the summer–autumn period of 2021. The positive direction of the wind velocity vectors corresponds to the north winds.

about 9 s. In the range of infragravity waves with periods from 25 to 250 s, there are many narrow-band wave processes, but significant energy peaks corresponding to the mode structure of infragravity waves are not distinguished.

In the density spectrum (Figure 3) in the range of minute sea level fluctuations for device 149, there is a peak at a period of about 10.7 min, and it exceeds the 95% confidence interval. In the spectrum of the second instrument 150, this peak is noticeable, but it is less than the confidence interval. Wave processes with such a period for the southeastern coast of Sakhalin was analyzed in the papers [*Kovalev and Kovalev*, 2017; *Kovalev et al.*, 2015]. It is shown that the oscillations detected in an open area of the coast with a period of about 10.7 minutes are trapped edge waves, and it is possible to expect an increase of oscillations at this period during dangerous marine phenomena, such as tsunami waves or storm surges. As our new measurements have shown, the peak value on the spectrum of the instrument 150 is much smaller and indicates that the edge wave exists from Cape Ostry to Cape Svobodny, after which it weakens, and perhaps does not spread further due to the steep bend of the coast.

Diagrams of the spectral density of level fluctuations, coherence and phase for long waves with periods from 10 min to tidal, are shown in Figure 4. Peaks exceeding 95%

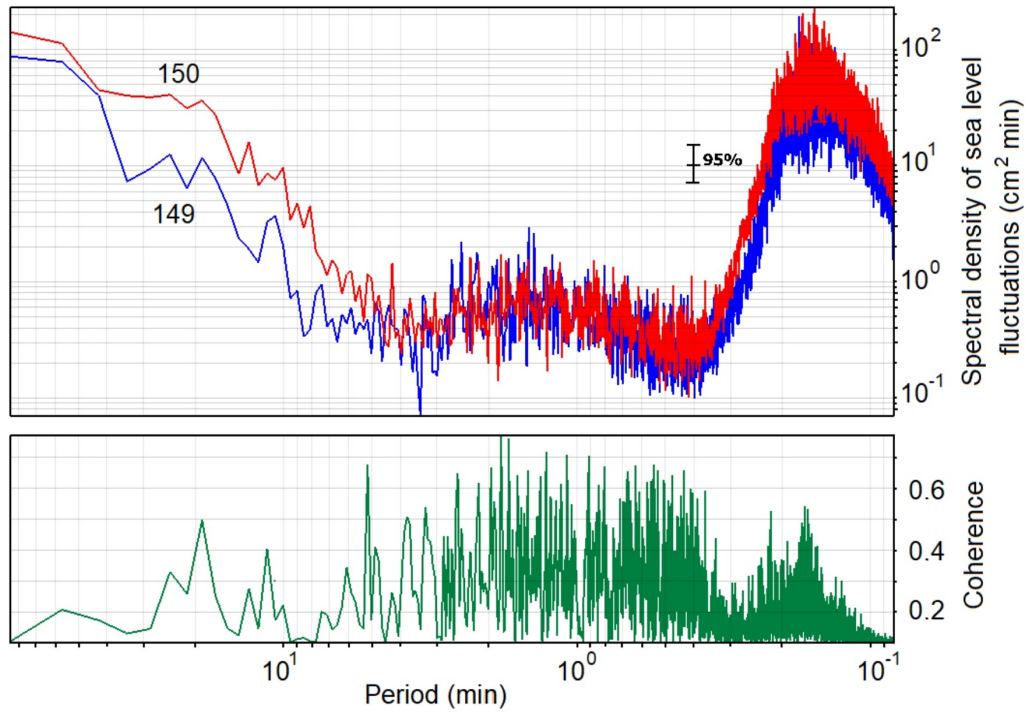

Figure 3. Diagram of the spectral density of sea level fluctuations for the period range of 5 s – 80 min.

confidence interval are distinguished in the spectra at periods close to: 24.63, 12.37, 8.25, 6.1, 4.1 hours and a group of peaks on periods from 0.55 to 1.85 hours.

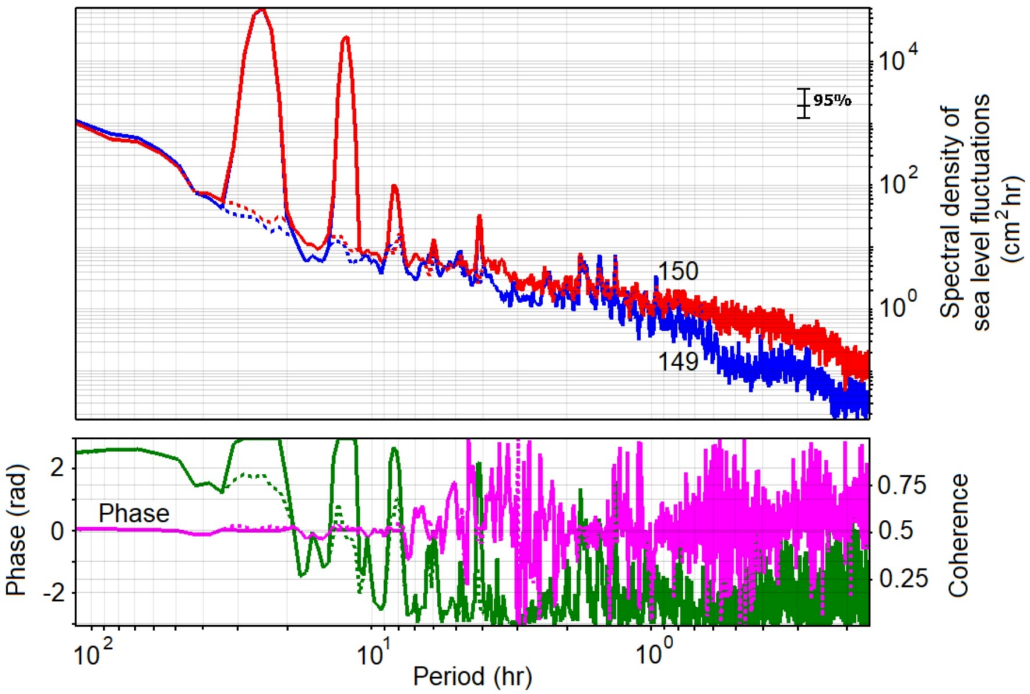

Figure 4. Diagrams of the spectral density of level, coherence and phase oscillations for long waves with periods from 10 minutes to 100 hours. The dotted lines refer to the time series from which the precalculated tide is subtracted.

In the marked part of the spectrum of the device 149, for a group of peaks with periods from 0.55 to 1.85 hours, only the three lowest-frequency ones exceed the confidence interval. And in the spectrum of the device 150, against the background of noise, only three peaks stand out at the same periods. It may indicate that these wave processes belong to seiches due to the peculiarities of local topography. Fluctuations with these periods are considered in the papers [*Kovalev and Kovalev*, 2018], where it is shown that they are really seiches, and fluctuations with a period of 1.52 h are shelf seiches.

In the long-wavelength part of the spectrum (Figure 4), peaks exceeding the 95% confidence interval at periods close to 24.63, 12.37, 8.25, 6.1, 4.1 hours. According to the data given in the paper [*Parker*, 2007] can be attributed, in accordance with the periods, to tidal harmonics in shallow water NO_1, NKS_2, NK_3, MK_4, $2MS_6$. At the same time, the spectral analysis of time series with the deducted precalculated tide confirmed that the detected peaks are tidal harmonics. We do not analyze them in detail here, but we note that attempts to divide two low-frequency waves into their tidal components, as was done in [*Squire et al.*, 2021], were unsuccessful and, consequently, mixed tidal harmonics are observed in the case under consideration.

4. Analysis of temperature fluctuations

Figure 5 shows diagrams of the spectral density of temperature fluctuations for a range of periods of 1–80 hours. Spectral peaks for 150 devices are located on periods of 25.5, 16.7, 12.9 and 6.7 hours. For the device 149 on periods of 13.2, 6.5, 5.3 hours. At the same time, coherence above the 95% confidence level of 0.4 is observed for oscillations with a period of 12.5 hours. Note that temperature fluctuations close to this period for devices 150 and 149 differ, which is clearly visible when the resolution of the spectrum increases.

The possible contribution of tidal components to the energy of internal waves was checked, for which the precalculated tide was subtracted from the temperature time series.

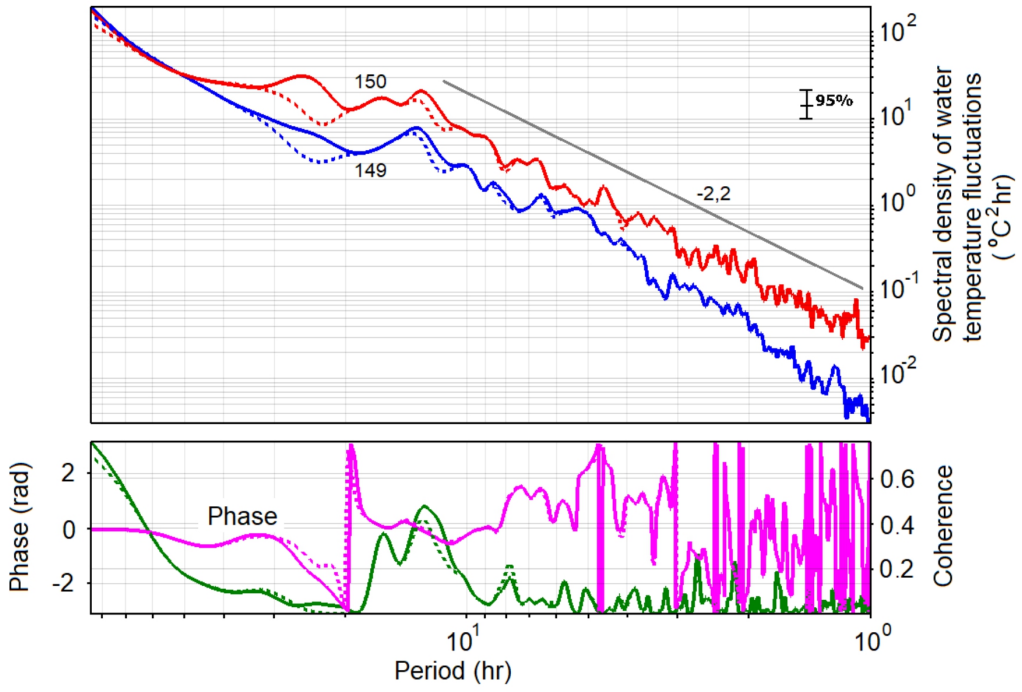

Figure 5. Diagrams of the spectral density of water temperature fluctuations, coherence and phase for the range of periods from 1 to 80 hours, calculated over the entire length of the time series. Sloping straight grey line is power-minus-two and two tenths curve. The dotted line marks the curves calculated for the time series with subtracted precalculated tide.

The spectra calculated from such series are shown in Figure 5 by dotted lines. It can be seen that the energy of tidal waves is transferred to internal waves at periods of about 24 hours. In addition, tidal oscillations with a semidiurnal period, as it were, mask internal waves with a period of about 13 hours. After subtracting the tides, oscillations with a period of about 13 hours stand out well in the spectra.

Also note that the periods of spectral peaks of water temperature fluctuations for periods longer than 5 hours do not coincide with the periods of peaks of sea level fluctuations, which means that these peaks of temperature fluctuations are determined by internal waves. In addition, in the spectrum of temperature fluctuations of device 150 (Figure 5) there are peaks at periods of 25.5, 16.7 hours (this period, as will be shown below, refers to the range of NI waves), and for device 149 in this range of peaks not highlighted.

At the beginning consider oscillations with a period of 25.5 hours. Shelf waves can be generated with such a period, but they were not detected in the spectra of level fluctuations (Figure 4). There may be two reasons for this. First, they may not be visible due to the closeness of their period to the period of the tidal harmonic, which has significant energy. Secondly, it is known that continental shelf waves make a relatively weak contribution to level fluctuations, but generate strong currents [*Cartwright*, 1969; *Cutchin and Smith*, 1973].

The possibility of the existence of shelf waves using model calculations was analyzed. It was taken into account that the installation latitude of the device 150 is about 46.85°E, then the inertial frequency $f = 2\Omega \sin\varphi$ where φ is the latitude, $\sin\varphi = 0.73$ and $\Omega = 7.2921 \times 10^{-5}\,\mathrm{s}^{-1}$ is the circular frequency of the Earth's rotation, we obtain $f = 1.06 \times 10^{-4}\,\mathrm{s}^{-1}$, and the period of inertial oscillations is 16.4 hours. Also note that shelf waves exist at frequencies below the inertial frequency $\omega < f$, while edge waves, on the contrary [*Rabinovich*, 1993], and they are caused by gyroscopic forces. And since the period of the waves, we observed is 25.5 hours, the frequency of which is $\omega = 0.0392\,\mathrm{cycle\,h}^{-1}$, then the ratio $\omega/f = 0.64$. It is for this ratio that the possibility of the existence of shelf waves is considered.

The dispersion relation for waves of the continental shelf was obtained by V. T. Buchwald and J. K. Adams in [*Buchwald and Adams*, 1968] for the exponential profile of the seabed on the shelf

$$\begin{cases} H(x) = h_0 e^{-2bx}, & 0 < x < L, \\ H(x) = D, & L < x < \infty, \end{cases} \tag{1}$$

where x is the sea coordinate, $H(x)$ is the shelf profile, the shelf width is $L = 115$ km, D is the sea depth, b is the coefficient in the exponent equal to $0.0205\,\mathrm{m}^{-1}$ for the bottom profile from Okhotskoe settlement. Note that the four parameters in equation (1) are related by the formula $D = h_0 e^{-2bL}$. Later, P. G. Leblon, L. A. Maysak and A. E. Gill generalized the theory, which are given in the papers [*Gill*, 1982; *LeBlond and Mysak*, 1978].

Using the approximation of the bottom profile in the area where the device 150 was installed, the dispersion diagram of shelf waves was calculated for different modes (from 0 to 4) of shelf waves using the formula given in [*Mysak*, 1980b]. The calculated dispersion diagram showed that for the detected wave period of 25.5 hours and the ratio $\omega/f = 0.64$, the existence of shelf waves of the first and second modes is possible. Such waves, according to [*LeBlond and Mysak*, 1978], are trapped by the shelf and propagate as a sequence of horizontal eddies with a variable sign, and they can be both barotropic and baroclinic. Such shelf waves, represented as eddies, as a result of interaction with islands, coastal currents, and due to the baroclinic instability considered in [*Darelius et al.*, 2009], can generate shorter wave processes that stand out in the spectra. Thus, from the foregoing, it follows that Figure 5 for device 150, the spectral peak with a period of 25.5 hours corresponds to internal waves excited by shelf waves.

The diagram of the spectral density of temperature fluctuations calculated using the full length of the recorded time series, shown in Figure 5, does not give an idea of the existence of wave processes during the observation time. Therefore, the spectrograms of the density of temperature fluctuations and the coherence, shown in Figure 6, were calculated from the time series of devices 149 and 150. It is clearly seen that internal

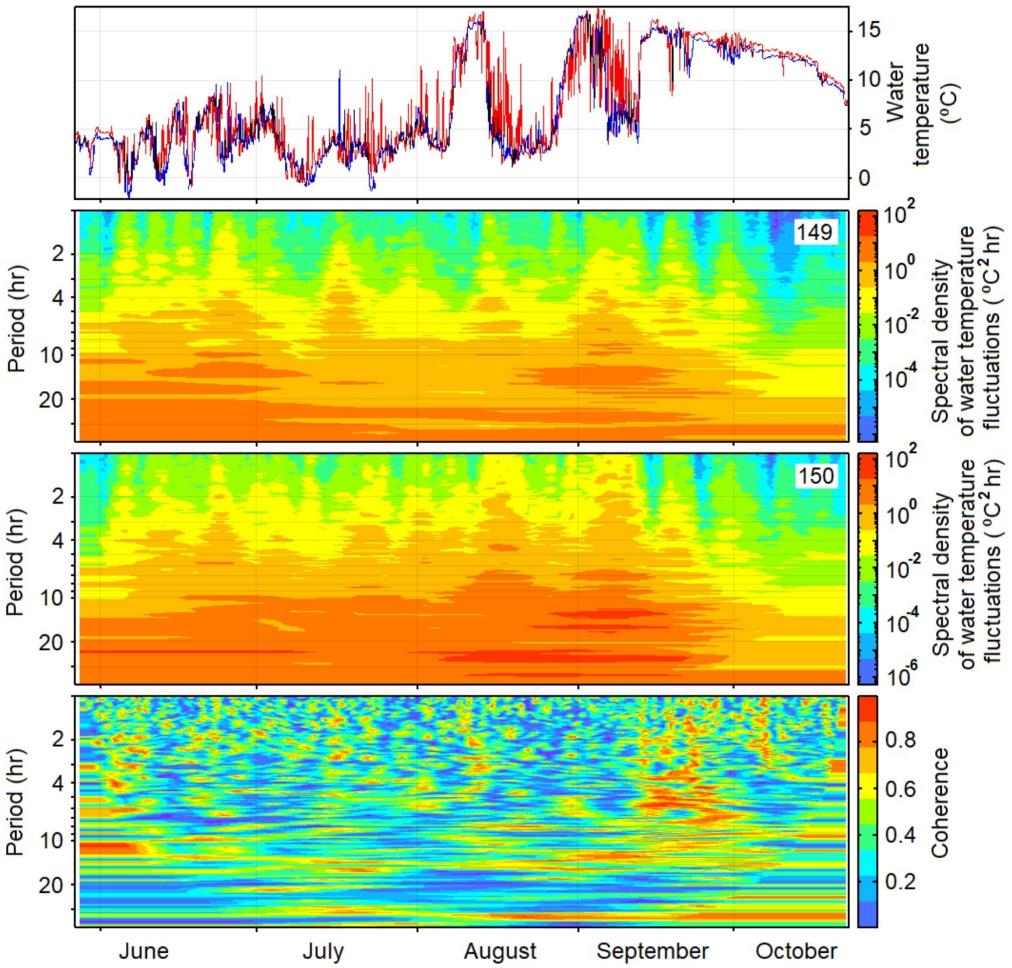

Figure 6. Spectrograms of temperature fluctuation density and coherence over time series of devices 149 and 150.

waves with periods of shelf waves of 25.5 hours, detected from the records of device 150, noticeably manifest themselves during significant temperature fluctuations from the second ten days of August to approximately September 20, sometimes reaching 10 °C. These wave processes are also visible on the spectrogram of the device 149, but their energy here is almost one and a half orders of magnitude lower, which probably can explain why they are not distinguished in the spectrum of device 149 in Figure 5.

Temperature fluctuations with a period of 16.7 hours, close to the inertial period of 16.4 hours, have the same trend as for periods of shelf waves. It can also be noted that with an increase in the temperature of the mixed layer from about mid-September, the energy of temperature fluctuations begins to gradually decrease and internal waves die out.

The coherence between the considered long-period temperature fluctuations, as can be judged from the coherence function in Figure 6 is not high. The exception is the waves observed in the second half of September, here a high degree of connection between the internal waves recorded by both devices is visible, moreover, from periods of 1 hour to 13 hours. Although the connection for wave periods of about 13 hours is observed sporadically at other times of observation.

In addition to the above, the wide rises in temperature in August and September attract attention (Figure 2b). As can be seen in Figure 2a,b, in August the rise coincides with the storm. The devices were at the sea bottom and there is no heating from solar radiation, and the uppermost layer is heated by the sun. And since mixing occurred during the storm, that is why there is a rather sharp increase in temperature near the bottom by

more than 10 °C. After the end of the storm, the mixing ceased, and the temperature at the sea bottom dropped.

The rise in temperature in late August – mid-September coincides with the peak of atmospheric pressure and long-lasting (about three days) southerly winds (Figure 7b,d). In our opinion, these winds contributed to the arrival of warm water from the south to the area where the devices were installed. The rise in temperature in mid-September is most likely due to a strong storm, which significantly mixed the water in the mixed layer, and therefore, after the end of the storm, the temperature did not drop sharply, but began to gradually decrease due the seasonal reduce of temperature. Also, on September 12 and 13, significant – up to 8–12 m s^{-1} winds of southern directions were observed (Figure 7d), which contributed to the arrival of a mass of warm water in the region.

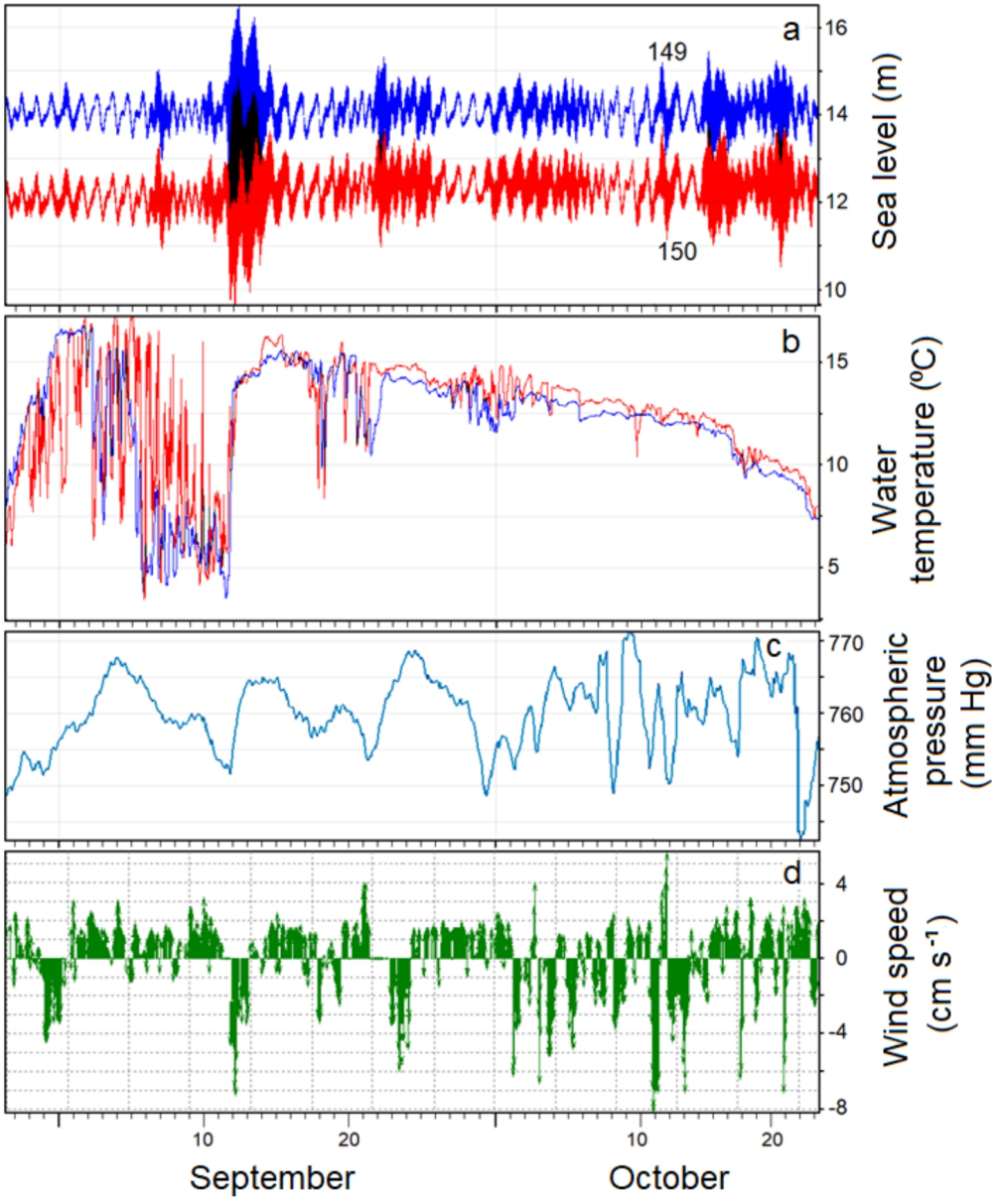

Figure 7. The time series of fluctuations in sea level (a), water temperature (b), atmospheric pressure (c) and wind speed (d) during September and October. The positive direction of the wind speed vectors corresponds to the northern winds.

Note that there is no rise in temperature after the storm at the end of May. This is apparently due to the fact that the upper layer of the sea has not yet been warmed up after the winter, taking into account the cold water coming from the north along the East Sakhalin Current.

5. Cyclone wakes

In Figure 2b it is clearly seen that in the second half of September, there are groups of waves on the temporary course of temperature fluctuations that appear sometime after the passage of cyclones. Since the presence of such wave packets, wakes of a cyclone were observed for the installation point of the device 150 and is discussed in the article [*Kovalev et al.*, 2022], but it used data from only one device for analysis, it seems appropriate to consider this phenomenon. For this purpose, time series with high resolution were constructed, shown in Figure 7. In Figure 7a,b it is clearly seen that after the passage of the cyclone and a significant decrease in the height of the waves on September 15, i.e. after 2 days, temperature fluctuations reaching 7 °C begin on the records of both devices. A similar picture, but with smaller temperature fluctuations in amplitude, is observed on September 28 after the waves after the next cyclone significantly decreased on September 26. For the device 150, there is still a one-time decrease in temperature on October 10.

Spectral analysis for the September–October period showed the presence of peaks in the spectra for device 150 for a period of about 13 hours and for device 149 with the same period. Note that for the observation point where the device 150 was installed in 2021, in 2020 the 2012 device also registered temperature fluctuations with periods of about 13 hours. The results of the analysis of these wave processes, given in [*Gill*, 1982], showed that wave processes with a period of about 13 hours belong to internal waves that form the so-called wake of a cyclone during relaxation after its passage.

Also note that in the papers [*Kunze*, 1985; *Teague et al.*, 2007], oscillations in the frequency range between $0.9f$ and $1.2f$ are defined as NI motions. As shown above, the period of inertial oscillations is 16.4 hours and the inertial frequency $f = 1.06{\times}10{\times}10^{-4}\,\mathrm{s}^{-1}$, for latitude 46°51′ – the installation location of the device 150. Then, according to E. Kunze, the periods of NI fluctuations are located between periods from 13.7 to 18.2 hours. The peak detected by us in the spectra with a period of 16.7 h located within this interval.

However, the period of 13 hours is shorter than the period of the lower boundary, i.e. the frequency of detected internal waves of the cyclone wake is slightly higher and does not located within the range of NI waves. In the paper [*Price et al.*, 1994], as well as in the case under consideration, the frequency of NI waves estimated by direct measurements turned out to be higher than the inertial frequency. At the same time, J. Price [*Price*, 1983] believes that the frequency of NI oscillations in a mixed layer is higher than the local inertial frequency by an amount approximately equal to half the Burger number of a mixed layer [*Price*, 1983; *Price et al.*, 1994].

According to [*Price*, 1983], the Burger number for a mixed layer is calculated by the equation:

$$B = (1 + 1/S^2)g'h_1/(2R_{\max})f)^2,$$

where $S = U_H/2Rf$ is the dimensionless velocity of the moving storm, $g' = g\Delta\rho/\rho_0$ and $\Delta\rho$ is the change in density, h_1 is the thickness of the mixed layer, $R_{\max}$ is the radius of the maximum pressure. And then, taking into account $R_{\max} \approx 40$ km, $f = 1.06{\times}10\times10^{-4}\,\mathrm{s}^{-1}$, $\Delta\rho = 4\,\mathrm{kg\,m}^{-3}$ [*Price*, 1983] and the fact that the lower boundary of the mixed layer in the Sea of Okhotsk from May to October does not go beyond 5–25 m (average 15 m) [*Tskhai*, 2017], obtain the value of the Burger number 0.32.

According to another equation $B = Nh_1/fR_{\max}$, where N is the Brunt-Väisälä frequency (in [*Kurkina et al.*, 2017], the value of the Brunt-Väisälä frequency near Sakhalin Island in July is given and its value varies from 0.01 to $0.038\,\mathrm{s}^{-1}$ with an average value of $0.025\,\mathrm{s}^{-1}$), obtain the Burger number $B = 0.31$ for the average thickness of a mixed layer of 15 m. The values of the Burger number obtained by different methods are close and slightly

differ from the one given in the paper [*Price*, 1983], in connection with the conclusion that the frequency of NI oscillations should be higher by an amount approximately equal to half of the Burger number for a mixed layer. Considering that the boundary of the upper frequency of the NI waves is $1.2f$ [*Kunze*, 1985; *Teague et al.*, 2007], then taking into account half of the Burger number equal to 0.155, we obtain the value of the upper boundary frequency of $1.37f$, and a period of 12.1 hours. Thus, the detected wave period about 13 hours can also be attributed to NI waves.

Since Cape Svobodny had two devices installed and the distance between them is known – 1.69 km on isobate, it is possible to determine the direction and the speed of wave propagation. Figure 8 shows the segments of the time series of water temperature for the time of the existence of the cyclone wake (Figure 8a) and in its absence (Figure 8b), when the winds of the southern direction were observed, the atmospheric pressure exceeded 760 mmHg, and the height of the waves at sea did not exceed 15 cm for the installation point device 150 and 10 cm for device 149.

It can be seen that during the existence of the cyclone wake, internal waves were first recorded by the device 150, and then 149. The difference in the time of arrival of the waves ranged from 46 to 130 min. Note that in the graph shown in Figure 5, there is also a phase difference between the waves recorded by the devices 149, 150 and is –0.052 rad (–2.98°). For calm weather, the time difference was 24–56 minutes. This means that the waves propagated in the direction from device 150 to device 149 and the propagation speed was 0.78–2.20 km h^{-1} for wake waves, and 1.81–4.22 km h^{-1} for internal waves of a calm sea. It is also clearly seen that the wave period of the cyclone wake is longer than for internal waves in calm weather. As follows from the spectral analysis, the period for wake waves is approximately 13 hours, and for internal waves in calm weather – 14.7 hours. It is possible that the difference in periods is because in the first case the waves are forced and in the second free.

It should be noted that the short length of the time series used for analysis in the paper [*Kovalev et al.*, 2022] did not allow us to draw two conclusions that can be concluded from long-term observations, namely: wakes of cyclones are formed when the water temperature of the mixed layer exceeds 10 °C. Also, temperature fluctuations with a period of about 13 hours – internal waves, are also present when cyclones do not move near the installation point of the devices and the water temperature is below 10 °C.

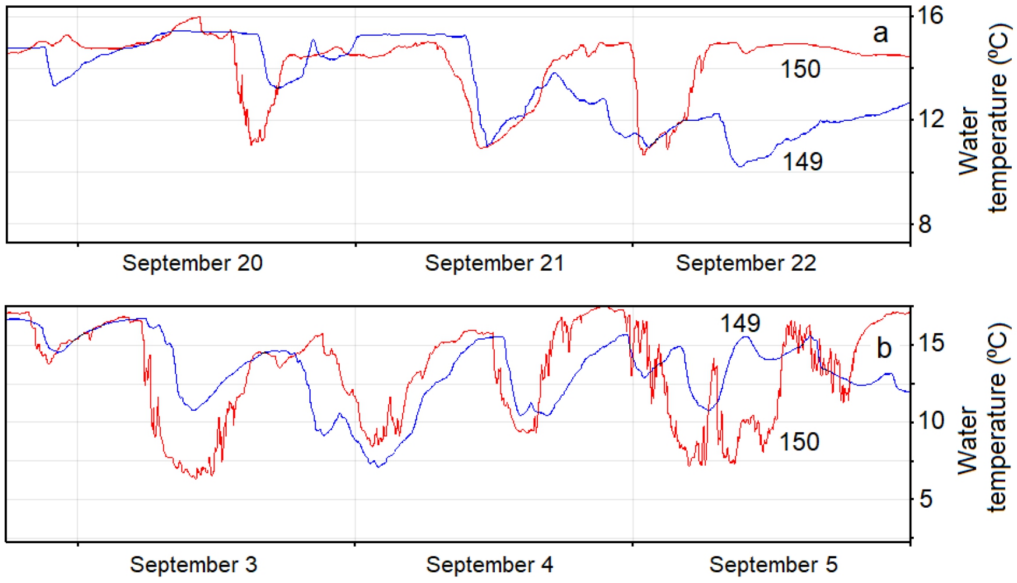

Figure 8. Segments of time series of water temperature for the time of existence of the cyclone wake (a) and in its absence (b).

6. Baroclinic instability

Above, the authors referred to the paper [*Darelius et al.*, 2009], who believes that shelf waves due to baroclinic instability can generate shorter wave processes that we observe. Baroclinic instability is a hydrodynamic instability that occurs in stably stratified rotating fluids and is ubiquitous in the Earth's atmosphere and oceans. It is often assumed that baroclinic instability is a mechanism that extracts potential energy stored in horizontal density gradients and uses this energy to create vortices [*Gill et al.*, 1974]. Baroclinic instability can lead to the formation of transient mesoscale vortices with a horizontal scale of 10 – 100 km [*George et al.*, 2021], and has a significant impact on weather and climate. Therefore, it is of interest to consider whether the manifestation of baroclinic instability is possible for the conditions of our observations.

The classical problems of baroclinic instability are considered in the papers [*Charney*, 1947; *Eady*, 1949] and are explained by the preferred scale of the length and growth rate of mesoscale disturbances observed in the ocean. These disturbances cover a significant part of the ocean depth and represent the subsidence of thermocline stratification under the influence of gravity and rotation. Many papers have been devoted to the study of baroclinic instability [*Boccaletti et al.*, 2007; *Smith*, 2007, 1976; *Swaters*, 1991]. It should be noted that the study of baroclinic instability is associated with the analysis of many parameters and modes, including the scale range under consideration, depends on the depth and therefore seems rather complicated. Therefore, in our paper, instability is considered using the results of the analysis of existing theoretical models set out in [*Cushman-Roisin and Beckers*, 2010; *Feng et al.*, 2021; *Vallis*, 2017] and others, and the possibility of occurrence of baroclinic instability for a specific water area is estimated.

In the paper [*Cushman-Roisin and Beckers*, 2010], the mechanism of baroclinic instability is considered using the thermal wind balance (also called baroclinic flux) due to geostrophic balance and hydrostatic balance, which maintain the flux in equilibrium. The presence of various waves will constantly perturb the existing flux with the thermal wind balance. When a disturbance with a favorable phase and wavelength appears, the system will irreversibly leave the equilibrium state and baroclinic instability will appear. To find the criterion for the manifestation of baroclinic instability, we use a simple linear model considered in the papers [*Cushman-Roisin and Beckers*, 2010; *Phillips*, 1954]. In model, the liquid consists of two layers of the same thickness $H/2$ and unequal density ρ_1 from above and ρ_2 from below, on the beta plane ($\beta_0 \neq 0$) above a flat bottom (at $z = 0$) and under a rigid lid (at $z = H$, const.). It is also assumed that the liquid is inviscid. The main flux is considered to be uniform horizontally and unidirectional, but with different speeds in each layer. For simplicity, the dynamics is chosen quasi-geostrophic, and a flat bottom and a hard rigid surface on top impose boundary conditions in the model and determine zero vertical velocity at these levels.

Without provide the initial equations and mathematical transformations set out in the paper [*Cushman-Roisin and Beckers*, 2010], let us turn to its conclusions. It is shown that it is the velocity difference $\Delta U = U_1 - U_2$ between the two layers, the vertical shift, that causes instability, and the phase velocity of the wave is real as long as the wave number k satisfies the condition:

$$R^4k^4(1 - r^4k^4) \leq (\beta_0 R^2/\Delta U^2)^2. \tag{2}$$

Here $R = \sqrt{g' \frac{H_1 H_2}{H_1+H_2}} = \frac{\sqrt{g'H}}{2f_0}$ is the baroclinic deformation radius, $g' = \frac{g(\rho_1-\rho_2)}{\rho_0}$, H_1, H_2 is the thickness of the upper and lower layers equal to $H/2$, f_0 is the Coriolis parameter at the equator in accordance with the beta plane approximation, $k = \sqrt{k_x^2 + k_y^2}$ is a two–dimensional wave number.

It is shown [*Cushman-Roisin and Beckers*, 2010] that the function $R^4k^4(1-R^4k^4)$ reaches a maximum of 1/4 for $Rk = (1/2)^{1/4} = 0.841$, and therefore the condition for perturbation of any wave number is satisfied if

$$|\Delta U| \leq 2\beta_0 R^2 = \beta_0 g' H/2f_0^2. \tag{3}$$

Thus, the system is stable to all small perturbations when the velocity shift ΔU is small enough not to exceed $2\beta_0 R^2$. In other words, the shift is destabilizing, because the greater the ΔU, the higher the probability that the threshold value will be exceeded. On the contrary, the beta effect stabilizes, because the greater the value of β_0, the higher the threshold value.

When the velocity shift exceeds the threshold value, condition (3) is not fulfilled, and not all wave numbers satisfy condition (2). Perturbations of the wave number k in the interval $k_{\min} < k < k_{\max}$ are unstable, where

$$k_{\min} = \left(\frac{1 - \sqrt{1 - 4\beta_0^2 R^4/\Delta U^2}}{2R^4} \right)^{1/4},$$

$$k_{\max} = \left(\frac{1 + \sqrt{1 - 4\beta_0^2 R^4/\Delta U^2}}{2R^4} \right)^{1/4}.$$

From equation (3) we see that instability on the beta plane can occur only with a sufficiently large shift ΔU. As ΔU increases, starting from a stable flow, the first instability occurs when $\Delta U = 2\beta_0 R^2$. At this shift level, the wavenumber of a single unstable mode is $k = 1/(2^{1/4}R) = 0.841/R$ and has a wavelength of

$$\lambda = 2\pi/k = 7.472R. \quad (4)$$

For $\Delta U > 2\beta_0 R^2$, the range of wavelengths and wave numbers ($k_{\min} < k < k_{\max}$) correspond to unstable waves, and the wavelength (4) does not belong to the fastest growing wave.

Finding the fastest growing wave is quite difficult due to the non-zero beta effect. To minimize the analysis, in the paper [*Cushman-Roisin and Beckers*, 2010], the consideration is limited to the plane f ($\beta_0 = 0$, which leads to $k_{\min} = 0$ and $k_{\max} = 1/R$), which is justified when considering shorter scales, more typical for the ocean than for the atmosphere. All perturbations of the wave number $k < 1/R$ are unstable, which corresponds to all wavelengths longer than $2\pi R$.

Let's estimate approximately the range of wave numbers for which the manifestation of baroclinic instability is possible. The reduced gravity coefficient g', which, taking into account $\Delta\rho = 4\,\mathrm{kg\,m^{-3}}$ taken from [*Alford*, 2003], $\rho_0 = 1020$–$1030\,\mathrm{kg\,m^{-3}}$, gives $g' = 0.038\,\mathrm{m\,s^{-2}}$. Since R, substituting the values $H = 50$ m, $f_0 = 1.7 \times 10^{-4}\,\mathrm{s^{-1}}$, we get $R = 4054.1$ m. Thus, all perturbations of the wave number $k < 1/R = 2.5 \times 10^{-4}\,\mathrm{m^{-1}}$ are unstable. Since the value of k obtained in the paper [*Kovalev et al.*, 2022] for the period of internal waves of 13 hours is equal to $1.9 \times 10^{-4}\,\mathrm{m^{-1}}$, this means that for waves with this period, and even more so for shelf waves having a significantly longer wavelength, baroclinic instability is possible.

7. Conclusions

Using two autonomous wave, temperature recorders and the Vantage Pro2™ weather station, five-month observations were carried out in the sea area near Cape Svobodny, south-east coast of Sakhalin (Russia) in 2021. As a result, records of fluctuations in sea level and water temperature with a one second discreteness were obtained. Atmospheric pressure and wind speed were recorded with hourly discreteness.

Spectral and cross-spectral analysis showed that in the density spectrum of the range of minute sea level fluctuations for the device 149, a peak exceeding the 95% confidence interval is allocated for a period of about 10.7 minutes. In the spectrum of the second device 150, this peak is noticeable, but it is less than the confidence interval. Thus, we confirmed the conclusions of the papers [*Kovalev and Kovalev*, 2017; *Kovalev et al.*, 2015] that the oscillations detected in an open area of the coast with a period of about 10.7 minutes are

trapped edge waves. Our measurements have shown that the edge wave existing from Cape Ostry to Cape Svobodny, just behind the Cape Svobodny weakens and this indicates that it does not spread further, possibly due to the steep bend of the coast.

Measurements of sea water temperature fluctuations for a range of periods of 1–80 hours were carried out. It is shown that since the periods of spectral peaks of water temperature fluctuations for periods longer than 5 hours do not coincide with the periods of peaks of sea level fluctuations, these peaks of temperature fluctuations are determined by internal waves.

The nature of temperature fluctuations with a period of 25.5 hours has been studied. It is shown that shelf waves can be generated with such a period. However, they are not detected in the spectra of sea level fluctuations and, perhaps, this is due to the fact that continental shelf waves include a relatively weak contribution to level fluctuations, but generate strong currents. At the same time, the analysis of the possibility of the existence of shelf waves using model calculations showed that the existence of shelf waves of the first and second modes is possible for the bottom relief of the water area under consideration. These waves, as a result of interaction with islands, coastal currents and baroclinic instability, can excite internal waves with a period of 25.5 hours. The calculated spectrogram of the density of temperature fluctuations showed that the internal waves detected by the records of the device 150 with shelf wave periods of 25.5 hours are noticeably manifested during significant temperature fluctuations from the second decade of August to about September 20, reaching at sometimes temperature 10 °C.

According to the time series of temperature fluctuations, the analysis of cyclones wakes was carried out. In addition to earlier studies of this phenomenon [*Kovalev et al.*, 2022], it was found that cyclone wakes form when the water temperature of the mixed layer exceeds 10 °C. It is also shown that internal waves with a period of about 13 hours are also present when cyclones do not move near the installation point of the devices and the water temperature is below 10 °C.

Using the density of water, the thickness of the mixed layer and the radius of the maximum cyclone wind for the observation area, the Burger number calculated, which allows correcting the range of near-inertial internal waves. Taking into account this correction, the temperature fluctuations detected in the density spectra with periods about 13 hours can be attributed to near-inertial fluctuations.

Using the results of a simple linear model considered in the papers [*Cushman-Roisin and Beckers*, 2010; *Phillips*, 1954], the possibility of baroclinic instability for periods of shelf waves is estimated. It is shown that baroclinic instability is possible for waves with a period of 13 hours, and even more so for period of shelf waves with a significantly longer wavelength.

Acknowledgements. The reported study was funded by the Ministry of Science and Higher Education of the Russian Federation (project No. FWWM-2021-0002) and Council of the grants of President of the Russian Federation for the state support of Leading Scientific Schools of the Russian Federation (Grant No. NSH-70.2022.1.5).

References

Alford, M. H. (2003), Improved global maps and 54-year history of wind-work on ocean inertial motions, *Geophysical Research Letters*, *30*(8), 1–4, https://doi.org/10.1029/2002gl016614.

Alford, M. H., J. A. MacKinnon, H. L. Simmons, and J. D. Nash (2016), Near-Inertial Internal Gravity Waves in the Ocean, *Annual Review of Marine Science*, *8*(1), 95–123, https://doi.org/10.1146/annurev-marine-010814-015746.

Boccaletti, G., R. Ferrari, and B. Fox-Kemper (2007), Mixed layer instabilities and restratification, *Journal of Physical Oceanography*, *37*(9), 2228–2250, https://doi.org/10.1175/jpo3101.1.

Buchwald, V. T., and J. K. Adams (1968), The propagation of continental shelf waves, *Proceedings of the Royal Society of London. Series A. Mathematical and Physical Sciences*, *305*(1481), 235–250, https://doi.org/10.1098/rspa.1968.0115.

Cartwright, D. E. (1969), Extraordinary Tidal Currents near St Kilda, *Nature*, *223*(5209), 928–932, https://doi.org/10.1038/223928a0.

Charney, J. G. (1947), The dynamics of long waves in a baroclinic westerly current, *Journal of Meteorology*, *4*(5), 136–162, https://doi.org/10.1175/1520-0469(1947)004<0136:tdolwi>2.0.co;2.

Cushman-Roisin, B., and J.-M. Beckers (2010), *Introduction to Geophysical Fluid Dynamics: Physical and Numerical Aspects*, 768 pp., Academic Press, London.

Cutchin, D. L., and R. L. Smith (1973), Continental Shelf Waves: Low-Frequency Variations in Sea Level and Currents Over the Oregon Continental Shelf, *Journal of Physical Oceanography*, *3*(1), 73–82, https://doi.org/10.1175/1520-0485(1973)003<0073:cswlfv>2.0.co;2.

Darelius, E., L. H. Smedsrud, S. Osterhus, A. Foldvik, and T. Gammelsrod (2009), Structure and variability of the Filchner overflow plume, *Tellus A*, *61*(3), 446–464, https://doi.org/10.1111/j.1600-0870.2009.00391.x.

D'Asaro, E. A. (1985), The Energy Flux from the Wind to Near-Inertial Motions in the Surface Mixed Layer, *Journal of Physical Oceanography*, *15*(8), 1043–1059, https://doi.org/10.1175/1520-0485(1985)015<1043:tefftw>2.0.co;2.

Eady, E. T. (1949), Long Waves and Cyclone Waves, *Tellus*, *1*(3), 33–52, https://doi.org/10.1111/j.2153-3490.1949.tb01265.x.

Efimov, V. V., E. A. Kulikov, A. B. Rabinovich, and I. V. Fine (1985), *Waves in the ocean boundary regions*, 280 pp., Hydrometeoizdat, Leningrad (in Russian).

Feng, L., C. Liu, A. Köhl, D. Stammer, and F. Wang (2021), Four Types of Baroclinic Instability Waves in the Global Oceans and the Implications for the Vertical Structure of Mesoscale Eddies, *Journal of Geophysical Research: Oceans*, *126*(3), 1–24, https://doi.org/10.1029/2020jc016966.

George, T. M., G. E. Manucharyan, and A. F. Thompson (2021), Deep learning to infer eddy heat fluxes from sea surface height patterns of mesoscale turbulence, *Nature Communications*, *12*(1), 800, https://doi.org/10.1038/s41467-020-20779-9.

Gill, A. E. (1982), *Atmosphere-Ocean Dynamics*, 662 pp., Elsevier Science & Technology Books, London.

Gill, A. E., J. S. A. Green, and A. J. Simmons (1974), Energy partition in the large-scale ocean circulation and the production of mid-ocean eddies, *Deep Sea Research and Oceanographic Abstracts*, *21*(7), 499–528, https://doi.org/10.1016/0011-7471(74)90010-2.

Gregg, M. C. (1987), Diapycnal mixing in the thermocline: A review, *Journal of Geophysical Research*, *92*, 5249, https://doi.org/10.1029/jc092ic05p05249.

Guan, S., W. Zhao, J. Huthnance, J. Tian, and J. Wang (2014), Observed upper ocean response to typhoon Megi (2010) in the Northern South China Sea, *Journal of Geophysical Research: Oceans*, *119*(5), 3134–3157, https://doi.org/10.1002/2013jc009661.

Kamenkovich, V. M. (1973), *Fundamentals of ocean dynamics*, 240 pp., Hydrometeoizdat, Leningrad (in Russian).

Kovalev, D. P. (2018), Certificate of state registration of computer programs no 2018618773 rf (in Russian).

Kovalev, D. P., and P. D. Kovalev (2017), Synchronization of Long Ocean Waves by Coastal Relief on the Southeast Shelf of Sakhalin Island, *International Journal of Bifurcation and Chaos*, *27*(13), 1750,195, https://doi.org/10.1142/s0218127417501954.

Kovalev, D. P., G. V. Shevchenko, and P. D. Kovalev (2015), Excitation of edge waves by atmospheric disturbances on the southeastern shelf of Sakhalin Island, in *Proceedings of the All-Russian Scientific Conference with international participation "Geodynamic processes and natural disasters. The experience of Neftegorsk"*, pp. 307–311, Dalnauka, Vladivostok (in Russian).

Kovalev, P. D., and D. P. Kovalev (2018), Long-wave processes on the southeastern shelf of Sakhalin Island, *Ecological Systems and Devices* (in Russian).

Kovalev, P. D., V. A. Squire, D. P. Kovalev, and A. I. Zaytsev (2022), Features of Formation of the Cyclone Wakes (Fluctuations in Seawater Temperature) in the Area of Cape Svobodny, the Southeastern Part of the Sakhalin Island, *Physical Oceanography*, *29*(1), 30–46, https://doi.org/10.22449/1573-160x-2022-1-30-46.

Kunze, E. (1985), Near-Inertial Wave Propagation In Geostrophic Shear, *Journal of Physical Oceanography*, *15*(5), 544–565, https://doi.org/10.1175/1520-0485(1985)015<0544:niwpig>2.0.co;2.

Kurkina, O. E., T. G. Talipova, T. Soomere, A. A. Kurkin, and A. V. Rybin (2017), The impact of seasonal changes in stratification on the dynamics of internal waves in the Sea of Okhotsk, *Estonian Journal of Earth Sciences*, *66*(4), 238–255, https://doi.org/10.3176/earth.2017.20.

LeBlond, P. H., and L. A. Mysak (1978), *Waves in the ocean*, 602 pp., Elsevier, Amsterdam.

Mysak, L. A. (1980a), Recent advances in shelf wave dynamics, *Reviews of Geophysics*, *18*(1), 211, https://doi.org/10.1029/rg018i001p00211.

Mysak, L. A. (1980b), Topographically Trapped Waves, *Annual Review of Fluid Mechanics*, *12*(1), 45–76, https://doi.org/10.1146/annurev.fl.12.010180.000401.

Parker, B. B. (2007), *Tidal analysis and prediction*, 378 pp., NOAA, NOS Center for Operational Oceanographic Products and Services, Maryland, https://doi.org/10.25607/OBP-191.

Phillips, N. A. (1954), Energy Transformations and Meridional Circulations associated with simple Baroclinic Waves in a two-level, Quasi-geostrophic Model, *Tellus*, *6*(3), 273–286, https://doi.org/10.1111/j.2153-3490.1954.tb01123.x.

Plekhanov, F. A., and D. P. Kovalev (2016), The complex program of processing and analysis of time-series data of sea level on the basis of author's algorithms, *Geoinformatics* (in Russian).

Pollard, R. T., and R. C. Millard (1970), Comparison between observed and simulated wind-generated inertial oscillations, *Deep Sea Research and Oceanographic Abstracts*, *17*(4), 813–821, https://doi.org/10.1016/0011-7471(70)90043-4.

Price, J. F. (1981), Upper Ocean Response to a Hurricane, *Journal of Physical Oceanography*, *11*(2), 153–175, https://doi.org/10.1175/1520-0485(1981)011<0153:uortah>2.0.co;2.

Price, J. F. (1983), Internal Wave Wake of a Moving Storm. Part I. Scales, Energy Budget and Observations, *Journal of Physical Oceanography*, *13*(6), 949–965, https://doi.org/10.1175/1520-0485(1983)013<0949:iwwoam>2.0.co;2.

Price, J. F., T. B. Sanford, and G. Z. Forristall (1994), Forced Stage Response to a Moving Hurricane, *Journal of Physical Oceanography*, *24*(2), 233–260, https://doi.org/10.1175/1520-0485(1994)024<0233:fsrtam>2.0.co;2.

Rabinovich, A. B. (1984), Topographic vortices in the area of the Kuril-Kamchatka trench, *Doklady USSR Academy of Sciences* (in Russian).

Rabinovich, A. B. (1993), *Long gravitational waves in the ocean: trapped, resonance, radiation*, 240 pp., Hydrometeoizdat, Leningrad (in Russian).

Sanford, T. B., J. F. Price, and J. B. Girton (2011), Upper-ocean response to Hurricane Frances (2004) observed by profiling EM-APEX floats, *Journal of Physical Oceanography*, *41*(6), 1041–1056, https://doi.org/10.1175/2010jpo4313.1.

Smith, K. S. (2007), The geography of linear baroclinic instability in Earth's oceans, *Journal of Marine Research*, *65*(5), 655–683, https://doi.org/10.1357/002224007783649484.

Smith, P. C. (1976), Baroclinic Instability in the Denmark Strait Overflow, *Journal of Physical Oceanography*, *6*(3), 355–371, https://doi.org/10.1175/1520-0485(1976)006<0355:biitds>2.0.co;2.

Squire, V. A., D. P. Kovalev, P. D. Kovalev, I. P. Medvedev, and M. E. Kulikov (2021), A cornucopia of oscillations on the Laptev Sea shelf, *Continental Shelf Research*, *227*, 104,514, https://doi.org/10.1016/j.csr.2021.104514.

Swaters, G. E. (1991), On the baroclinic instability of cold-core coupled density fronts on a sloping continental shelf, *Journal of Fluid Mechanics*, *224*, 361–382, https://doi.org/10.1017/s0022112091001799.

Teague, W. J., E. Jarosz, D. W. Wang, and D. A. Mitchell (2007), Observed oceanic response over the upper continental slope and outer shelf during hurricane Ivan, *Journal of Physical Oceanography*, *37*(9), 2181–2206, https://doi.org/10.1175/jpo3115.1.

Tskhai, Z. R. (2017), *Spatial and temporal variability of chlorophyll-a concentration in the surface layer of the Sea of Okhotsk and adjacent water areas according to satellite data*, 157 pp., Publishing house of the Shirshov Institute of Oceanology of Russian Academy of Sciences, Moscow.

Vallis, G. K. (2017), *Atmospheric and Oceanic Fluid Dynamics. Fundamentals and Large-Scale Circulation*, 946 pp., Cambridge University Press, https://doi.org/10.1017/9781107588417.

Yang, B., Y. Hou, P. Hu, Z. Liu, and Y. Liu (2015), Shallow ocean response to tropical cyclones observed on the continental shelf of the northwestern South China Sea, *Journal of Geophysical Research: Oceans*, *120*(5), 3817–3836, https://doi.org/10.1002/2015jc010783.